Exploring Spatial Flexibility and Phase Design in Fluid Reconfigurable Intelligent Surfaces: A Physical Layer Security Perspective

J. D. Vega-Sánchez, *Senior Member, IEEE*, V. H. Garzón Pacheco, N. V. Orozco Garzón, *Senior, IEEE*, D. A. Riofrío Almeida, *Member, IEEE*, and D. P. Moya Osorio, *Senior Member, IEEE*

Abstract—This work examines the secrecy outage probability (SOP) in Fluid Reconfigurable Intelligent Surfaces (FRIS) and contrasts their performance against two alternative RIS architectures: a traditional planar RIS and a compact RIS layout. To characterize the end-to-end FRIS channel, a maximum likelihood estimation (MLE) approach is introduced, while a Q-learning algorithm is employed to adaptively select the spatial positions of FRIS elements. Numerical evaluations show that optimizing element placement in FRIS significantly improves SOP compared to conventional RIS without phase adaptation. However, these improvements become less evident once the conventional RIS implements optimized beamforming (BF) and phase-shift (PS) controlling. In addition, FRIS maintains a clear advantage over compact RIS designs with optimized BF and PS, mainly due to its lower spatial correlation. Results further indicate that reducing the inter-element distance negatively impacts SOP, highlighting the importance of spatial diversity.

Index Terms—Fluid reconfigurable intelligent surfaces, secrecy outage probability, q-learning.

I. INTRODUCTION

Reconfigurable Intelligent Surfaces (RISs) have emerged as a promising approach for achieving cost-effective and energyefficient control of the radio environment. By leveraging nearly passive reflecting elements with tunable phase shifts, RISs can reshape wireless channels to allow gains in coverage and performance, especially in scenarios where direct links are severely weakened or blocked [1]. Despite their potential, conventional RIS implementations are limited by spatial correlation, discrete phase constraints, restricted degrees-offreedom (DoF), and control overhead. These issues may limit their performance in practice. Despite their potential, conventional RIS implementations are limited by spatial correlation, discrete phase constraints, and restricted degrees-of-freedom (DoF), and control overhead associated with configuring a large number of reflecting elements. These issues may limit their performance in practice.

Considering the potential advantages of RIS, the concept of fluid reconfigurable intelligent surfaces (FRISs) has recently

Manuscript received MONTH xx, YEAR; revised XXX. The review of this paper was coordinated by XXXX.

(Corresponding author: José David Vega-Sánchez)

been introduced [2]. Unlike fixed-layout RISs, FRIS allows the reflecting elements to physically relocate within predefined subregions, adding spatial position optimization as a new DoF. This flexibility enables FRIS to significantly improve achievable rates, sensing performance, and interference management compared to conventional RISs. Furthermore, extensions such as Fluid Integrated Reflecting and Emitting Surfaces (FIRES) broaden the range of applications by combining reflection and emission functionalities [3]. In parallel, the study of FRIS within the context of physical layer security (PLS) has gained increasing attention, motivated by the inherent advantages of movable antennas in enhancing secrecy performance. For instance, the work in [4] analyzed the fundamental principles and achievable secrecy rates of movable antennas under different channel conditions. In [5], the authors investigated the secrecy outage probability (SOP) and demonstrated that spatial adjustment effectively mitigates eavesdropping. The approach in [6] provided a statistical analysis showing the overall secrecy gains achievable through movement diversity. Such works highlight that, while movable or fluid antennas can exploit spatial randomness to enhance PLS, their benefits come at the cost of increased control and channel estimation overhead. In parallel, the study of FRIS within the context of physical layer security (PLS) has gained increasing attention, motivated by the inherent advantages of movable antennas in enhancing secrecy performance [4–6]. By dynamically adjusting element positions, FRIS can exploit spatial randomness to reduce the information leakage towards eavesdroppers, thereby lowering the secrecy outage probability (SOP). Such advantages become particularly relevant in scenarios where traditional RISs face limitations due to strong spatial correlation.

Motivated by these developments, this paper investigates the SOP performance of FRIS-assisted systems under full optimization of spatial positions, beamforming (BF), and phase shifts (PS). In contrast to previous works that rely on statistical approximations or unsupervised clustering-based methods for channel modeling [1], we adopt a closed-form maximum likelihood estimation (MLE) framework to characterize the endto-end channel. Moreover, we employ a Q-learning algorithm to efficiently optimize the element positions of FRIS, while BF and PS are designed through a distributed optimization scheme. Our results reveal that although FRIS provides significant SOP gains compared to conventional RIS without phase optimization, such benefits diminish when conventional RIS employs fully optimized BF and PS. Nevertheless, FRIS consistently outperforms compact RIS architectures due to its

J. D. Vega-Sánchez is with the Colegio de Ciencias e Ingenierías "El Politécnico", Universidad San Francisco de Quito (USFQ), Diego de Robles S/N, Quito (Ecuador) 170157.

V. H. Garzón Pacheco and N. V. Orozco Garzón are with the Faculty of Engineering and Applied Sciences (FICA), Telecommunications Engineering, Universidad de Las Américas (UDLA), Quito 170124, Ecuador.

D. P. Moya Osorio is with Communication Systems Division, Department of Electrical Engineering, Linköping University, 581 83 Linköping, Sweden.

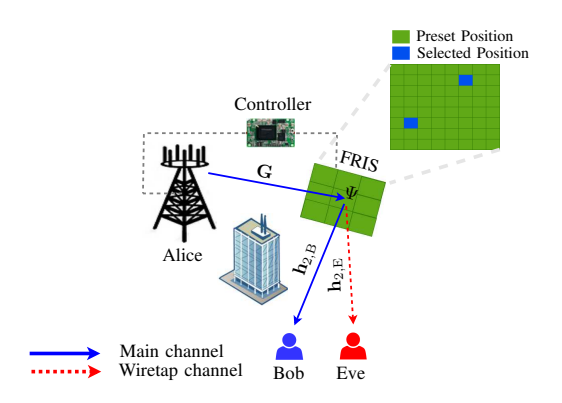


Fig. 1. System model for FRIS-enabled communication.

reduced spatial correlation, and we further demonstrate that SOP degrades as the inter-element spacing decreases.

Notation and terminology: Uppercase and lowercase bold letters denote matrices and vectors, respectively; $f(\cdot)$ is a probability density function (PDF); $F_{(\cdot)}(\cdot)$ is a cumulative density function (CDF); $\mathcal{CN}(\cdot,\cdot)$ is the circularly symmetric complex Gaussian distribution; $J_0(\cdot)$ is the zeroth-order Bessel function of the first kind; $(\cdot)^{H}$ is the Hermitian transpose; $(\cdot)^{T}$ is the transpose.

II. SYSTEM AND CHANNEL MODELS

We consider a Fluid RIS (FRIS)-assisted wiretap system with a transmitter Alice (A) equipped with L antennas, a single-antenna legitimate receiver Bob (B), and a singleantenna eavesdropper Eve (E). Direct line-of-sight links from A to B or E are blocked, so communication relies on the FRIS (see Fig. 1). The FRIS surface has area $A_T = NA_p$ in m^2 , where $N = N_v N_h$ is the number of preset positions uniformly arranged in an $N_v \times N_h$ grid. Also, $A_p = d_H d_V$ denotes the area of each FRIS unit, with $d_{\rm H}$ and $d_{\rm V}$ being its horizontal width and vertical height, respectively, thus defining the physical footprint of each element. Each preset position is represented by $\mathbf{c}_n = [c_{x,n}, c_{y,n}]^T$, and the complete candidate set is $\mathcal{C} = \{\mathbf{c}_1, \dots, \mathbf{c}_N\}$. The surface is partitioned into M disjoint subareas $\{S_1, \dots, S_M\}$, each assigned to one active fluid element that is restricted to move freely within its own subarea, but only among the N/M discrete preset positions arranged as a local 2D grid. The position of the m-th element is $\mathbf{p}_m = [p_{x,m}, p_{y,m}]^{\mathrm{T}}$, and the overall active configuration is $\mathcal{P} = [\mathbf{p}_1, \dots, \mathbf{p}_M]$, i.e., M elements selected out of N. The received signal at B or E depends on the chosen configuration \mathcal{P} and is expressed as

$$y_{i,(\mathcal{P})} = \sqrt{P} \mathbf{h}_{2,i}^{\mathbf{H}} \mathbf{\Psi}_{(\mathcal{P})} \mathbf{G}_{(\mathcal{P})} \mathbf{w} x + n_i, \tag{1}$$

where $i \in \{B, E\}$ denotes either the legitimate or eavesdropper channels, P is the transmit power at A, x the transmitted signal, and $n_i \sim \mathcal{CN}(0, \sigma_i^2)$ the the additive white Gaussian noise with variance σ_i^2 . The maximum ratio transmission (MRT) BF vector at \mathbf{A} is \mathbf{w} , while $\mathbf{G}_{(\mathcal{P})} = [\mathbf{g_1}, \dots, \mathbf{g_L}] \in \mathbb{C}^{M \times L}$ and $\mathbf{h}_{2,i} = [h_{2i,1}, \dots, h_{2i,M}]^H \in \mathbb{C}^{M \times 1}$ denote the A-to-FRIS and FRIS-to-i channels, respectively. The FRIS phase-shift matrix is $\Psi_{(P)} = \operatorname{diag}(e^{j\phi_1}, \dots, e^{j\phi_M})$, assuming no reflection loss. Each element aligns its phase toward B as $\phi_m = -\angle(h_{2,\mathrm{B},m}^\mathrm{H}) - \angle(\mathbf{g}_m \mathbf{w})$, with $h_{2,\mathrm{B},m}^\mathrm{H}$ the m-th entry of $\mathbf{h}_{2.\mathrm{B}}^{\mathrm{H}}$ and \mathbf{g}_m the m-th row of $\mathbf{G}_{(\mathcal{P})}$. The pair (\mathbf{w}, ϕ_m) is optimized to maximize the end-to-end SNR at B. All FRIS links are modeled as Rayleigh fading with spatial correlation. Hence, $\mathbf{h}_{2,i} \sim \mathcal{CN}(\mathbf{0}_N, A_p \beta_{2,i} \mathbf{R}_{(\mathcal{P})})$ and $\mathbf{g}_m \sim \mathcal{CN}(\mathbf{0}_M, A\beta_1 \mathbf{R}_{(\mathcal{P})}), \text{ for } m \in \{1, \dots, M\}, \text{ where }$ β_1 and $\beta_{2,i}$ denote the path-loss factors of the A-to-FRIS and FRIS-to-i links. The correlation matrix $\mathbf{R}_{(\mathcal{P})} \in \mathbb{C}^{M \times M}$ follows Jake's model under rich scattering, so that its (a, b)-th entry is

$$\begin{bmatrix} \mathbf{R}_{(\mathcal{P})} \end{bmatrix}_{a,b} = J_0 \left(2 \left\| \mathbf{u}_a - \mathbf{u}_b \right\| / \lambda \right) \quad a,b = 1,\ldots,M, \qquad (2)$$
 where λ is the carrier wavelength, $\mathbf{u}_\zeta = [0, \operatorname{mod}(\zeta - 1, M_h) \, d_{\mathrm{H}}, \, \lfloor (\zeta - 1) / M_v \rfloor \, d_V \rfloor^T$ with $\zeta \in \{a, b\}$. Here, M_h and M_v represent the numbers of selected FRIS positions along the horizontal and vertical dimensions of the metasurface, respectively, so that $M = M_h \times M_v$. Based on these definitions and (1), the received signal-to-noise ratio (SNR) at both B and E can be written as

$$\gamma_{i,(\mathcal{P})} = \overline{\gamma}_i |\mathbf{h}_{2,i}^{\mathrm{H}} \mathbf{\Psi}_{(\mathcal{P})} \mathbf{G}_{(\mathcal{P})} \mathbf{w}|^2, \tag{3}$$

where, we define $\overline{\gamma}_i = P/\sigma_i^2$ as the average transmit SNR for

III. PROBLEM FORMULATION AND ALGORITHM DESIGN A. Problem Formulation

Here, the goal is to choose the most suitable M positions out of the total N preset candidates distributed over the FRIS surface so as to maximize the received SNR at B. Formally, let the complete set of N candidate positions be $\mathcal{C} = \{\mathbf{c}_1, \mathbf{c}_2, \dots, \mathbf{c}_N\}$, from which we define a subset $\mathcal{P} \subset \mathcal{C}$ with cardinality $|\mathcal{P}| = M$, representing the positions of the M active fluid elements. Accordingly, the optimization problem can be expressed as:

(P1):
$$\max_{\mathcal{P} \subset \mathcal{C}, \, |\mathcal{P}| = M} \gamma_{i,(\mathcal{P})}$$
(4a)
s.t.
$$\mathbf{p}_m \in \mathcal{S}_m, \quad \forall m = 1, \dots, M,$$
 (4b)

s.t.
$$\mathbf{p}_m \in \mathcal{S}_m, \quad \forall m = 1, \dots, M,$$
 (4b)

$$\|\mathbf{p}_m - \mathbf{p}_{m'}\|_2 \ge D, \quad \forall m \ne m',$$
 (4c)

where $\mathbf{p}_m \in \mathbb{R}^2$ denotes the two-dimensional coordinate of the m-th selected fluid element, and the index m' corresponds to another element different from m. Constraint (4c) ensures that a minimum separation distance D is maintained between elements, thereby preventing electromagnetic coupling or physical overlap.

B. Optimization Algorithm Design

1) Q-Learning for Position Selection: Due to the nonconvexity of problem (P1), conventional methods may not reach the global optimum. Hence, we adopt a Q-learning scheme [7], where the FRIS controller acts as the agent, the states represent the spatial configuration of the fluid elements, and the actions correspond to selecting new positions from C. The environment provides a reward defined as the end-to-end SNR at B, and the Q-table is updated iteratively. The update rule for a state-action pair (s, a) at iteration t is:

$$Q_{t+1}(s, a) = Q_t(s, a) + \alpha \Big[r + \delta \max_{a'} Q_t(s', a') - Q_t(s, a) \Big],$$
(5)

Algorithm 1 Q-Learning-Based Position Optimization for **FRIS**

```
1: Input: Total area A_T = [X_{\min}, X_{\max}] \times [Y_{\min}, Y_{\max}], number of fluid elements M, minimum spacing D, power P, maximum episodes E, maximum steps per
      episode T, learning rate \alpha, discount factor \delta, exploration probability \epsilon.
2: Initialization: Initialize Q-table Q(s, a) with zeros for all states s and actions a.
     Partition the FRIS surface into M subareas \{S_1,\ldots,S_M\} with spacing \geq D. Precompute channels: A-to-FRIS \mathbf{G} \in \mathbb{C}^{N \times L}, FRIS-to-B \mathbf{h}_{2,\mathrm{B}} \in \mathbb{C}^{N \times 1}, and correlation matrix \mathbf{R} \in \mathbb{C}^{N \times N}.
3: for each episode e = 1 to E do
          Initialize state s_0 with random positions \mathcal{P}^{(0)} = \{\mathbf{p}_1^{(0)}, \dots, \mathbf{p}_M^{(0)}\} within
           for each step t = 1 to T do
6:
                 Select action a_t (new position for one element) using an \epsilon-greedy policy
```

from $Q(s_t, a)$

7: Apply action a_t to obtain the new configuration $\mathcal{P}^{(t)}$ and the corresponding

Evaluate reward r_t as the received SNR $\gamma_{B,(\mathcal{P}^{(t)})}$ based on (3). 8: 9.

Update Q-table using (5).

10: if termination criterion is satisfied (e.g., convergence of $\mathcal P$ or maximum

11: 12: 13: end for 14: end for

15: Final greedy selection: Starting from an empty configuration, sequentially select for each subarea S_m the action $a^* = \arg \max_a Q(s, a)$, ensuring feasibility with respect to the spacing constraint D. The resulting configuration is denoted by \mathcal{P}'

16: **Output:** Optimized configuration $\mathcal{P}^* = \{\mathbf{p}_1^*, \dots, \mathbf{p}_M^*\}$ with maximum reward $\gamma_{\mathbf{B}, (\mathcal{P}^*)}$ with final dimensions: $\mathbf{G} \in \mathbb{C}^{M \times L}, \mathbf{R} \in \mathbb{C}^{M \times M}, \mathbf{h}_{2,\mathbf{B}} \in \mathbb{C}^{M \times 1}$..

where $\alpha \in (0,1]$ is the learning rate, $\delta \in [0,1]$ is the discount factor, r is the immediate reward, s' is the next state, and $\max_{a'} Q_t(s', a')$ denotes the maximum Q-value attainable from the new state. Algorithm 1 outlines the proposed Qlearning-based procedure for optimizing the spatial configuration of the FRIS fluid elements.

2) Distributed Phase Shift and Beamforming Optimization: After obtaining the optimal set of positions \mathcal{P}^{\star} , we proceed to the joint optimization of the transmit BF vector at node A and the PS of the active FRIS elements. The corresponding problem is expressed as

(P2):
$$\max_{\mathbf{w}, \Psi_{(\mathcal{P}^{\star})}} \gamma_{\mathbf{B}, (\mathcal{P}^{\star})}$$
 (6a)

s.t.
$$\|\mathbf{w}\|^2 \le P_{\text{max}},$$
 (6b)

$$0 \le \phi_m < 2\pi, \quad \forall m = 1, \dots, M, \tag{6c}$$

where $\gamma_{\mathrm{B},(\mathcal{P}^{\star})}$ denotes the end-to-end SNR at B given the fixed configuration \mathcal{P}^* . To solve (P2), we adopt a distributed alternating optimization method [8]. In this approach, the transmit BF at A and the phase shifts at the FRIS are updated iteratively: in each iteration one variable is optimized while the other remains fixed, and the procedure continues until convergence or until a maximum number of iterations is attained. The proposed FRIS-specific algorithm is summarized in Algorithm 2. Finally, upon solving (P1) and (P2), the received in both B and E can be written as

$$y_{i,(\mathcal{P}^{\star})} = \sqrt{P} \,\mathbf{h}_{2,i}^{\mathrm{H}} \mathbf{\Psi}_{(\mathcal{P}^{\star})}^{\star} \mathbf{G}(\mathcal{P}^{\star}) \,\mathbf{w}^{\star} x + n_{i}. \tag{7}$$

Notice that $\Psi_{(\mathcal{P}^{\star})}^{\star}\mathbf{G}(\mathcal{P}^{\star})\mathbf{w}^{\star}$ corresponds to the fully optimized end-to-end link towards B. Consequently, the received SNR in both B and E nodes is given by

$$\gamma_{i,(\mathcal{P}^{\star})} = \overline{\gamma}_{i} \left| \mathbf{h}_{2,i}^{\mathrm{H}} \mathbf{\Psi}_{(\mathcal{P}^{\star})}^{\star} \mathbf{G}(\mathcal{P}^{\star}) \mathbf{w}^{\star} \right|^{2} = \overline{\gamma}_{i} \left| h_{i}^{\star} \right|^{2}, \quad (8)$$

where h_i^{\star} denotes the equivalent end-to-end FRIS channel after optimization.

Algorithm 2 Distributed Phase Shift and Beamforming Optimization

```
1: Initialize tolerance \tau>0 and iteration index k=1.
2: BF initialization: Estimate \mathbf{G}_{(\mathcal{P}^\star)}\in\mathbb{C}^{M\times L} and set \mathbf{w}^{(k)}=\mathbf{1}_L/\sqrt{L}\in
         PS update: With \mathbf{w}^{(k)} fixed, compute \phi_m^{(k+1)} = -\angle(h_{2,\mathrm{B},m}^\mathrm{H}) - \angle(\mathbf{g}_m\mathbf{w}^{(k)}), and set \Psi_{(\mathcal{P}^\star)}^{(k+1)} = \mathrm{diag}\left(e^{j\phi_1^{(k+1)}},\ldots,e^{j\phi_M^{(k+1)}}\right).
                  BF update: With \Psi_{(\mathcal{P}^{\star})}^{(k+1)} fixed, update \mathbf{w}^{(k+1)} = \frac{\left(\mathbf{h}_{2,\mathrm{B}}^{\mathrm{H}}\Psi_{(\mathcal{P}^{\star})}^{(k+1)}\mathbf{G}_{(\mathcal{P}^{\star})}\right)^{\mathrm{H}}}{\left\|\mathbf{h}_{2,\mathrm{B}}^{\mathrm{H}}\Psi_{(\mathcal{P}^{\star})}^{(k+1)}\mathbf{G}_{(\mathcal{P}^{\star})}\right\|}
7: until fractional increase in \gamma_{\rm B}(\mathcal{P}^{\star}) < \tau or maximum iterations reached
8: Output: Optimized \mathbf{w}^* and \Psi_{(\mathcal{P}^*)}^*.
```

IV. PERFORMANCE ANALYSIS

A. Approximate SNR Distributions

Here, we employ the Maximum Likelihood Estimation (MLE) method to approximate the PDFs of the magnitude $|h_i^{\star}|$ with a single distribution, denoted as $H_i \sim \text{Nakagami}(\varphi_i =$ $\{\Omega_i, m_i\}$), where Ω_i denotes the average power and m_i is the fading parameter. Let us then consider a training set vector $\mathbf{h}_{i}^{\star} = \{h_{i,j}^{\star}\}_{j=1}^{t_{sp}}$, consisting of t_{sp} independent samples of h_{i}^{\star} obtained from (8). The parameter vector φ_i is estimated by maximizing the log-likelihood function $L(H_i \mid \varphi_i)$ associated with the PDF of H_i , based on the sample data set \mathbf{h}_i^{\star} . Accordingly, following [9], the log-likelihood function is expressed

$$L(H_i \mid \boldsymbol{\varphi}_i) = \sum_{j=1}^{t_{sp}} \log [f_H(h_{i,j}^{\star}; \boldsymbol{\varphi}_i)].$$
 (9)

Then, the parameter estimates are obtained by setting the gradient of $L(H_i \mid \varphi_i)$ with respect to each parameter to zero. Thus, the MLE estimator of an entry $\varphi_{i,t} \in \varphi_i$, with $t \in \{1, 2\}$, is given by

$$\frac{\partial L(H_i \mid \boldsymbol{\varphi}_i)}{\partial \varphi_i, t} = \sum_{j=1}^{t_{sp}} \frac{\partial}{\partial \varphi_i, t} \log \left[f_{H_i} \left(h_{i,j}^{\star}; \boldsymbol{\varphi}_i \right) \right] = 0. \quad (10)$$

Proposition 1. Once the parameter vector φ_i is estimated with MLE, the PDF of $H_{\rm E}$ and the CDF of $H_{\rm B}$ of the received SNR can be approximated using a Gamma distribution via $\gamma_{i,(\mathcal{P}^*)} = \overline{\gamma}_i |H_i|^2$. So, the corresponding expressions are given

$$f_{\gamma_{\mathrm{E},(\mathcal{P}^{\star})}}(\gamma_{E}) = \frac{\gamma_{E}^{k_{E}-1}}{\Gamma(k_{E})\,\overline{\gamma}_{\mathrm{E}}\,\theta_{E}^{k_{E}}} \exp\left(-\frac{\gamma_{E}}{\overline{\gamma}_{\mathrm{E}}\theta_{E}}\right),\qquad(11)$$

$$F_{\gamma_{\mathrm{B},(\mathcal{P}^{\star})}}(\gamma_{\mathrm{B}}) = \frac{\Upsilon\left(k_{\mathrm{B}},\frac{\gamma_{\mathrm{B}}}{\overline{\gamma}_{\mathrm{B}}\theta_{\mathrm{B}}}\right)}{\Gamma(k_{\mathrm{B}})},$$

where $k_i = m_i$, and $\theta_i = \frac{\Omega_i}{m_i}$, with

$$\Omega_i = \frac{1}{t_{sp}} \sum_{j=1}^{t_{sp}} (h_{i,j}^{\star})^2 \quad \text{(a)}, \qquad m_i = \frac{1 + \sqrt{1 + \frac{4\Delta_i}{3}}}{4\Delta_i} \quad \text{(b)},$$
(12)

in which Δ_i is given by (16).

B. Secrecy Outage Probability

We consider a passive wiretap scenario where the eavesdropper's CSI is unavailable at Alice. Hence, Alice transmits with a fixed secrecy rate $R_{\rm S}$. The secrecy capacity is defined as $C_{\rm S} = \max\{C_{\rm B} - C_{\rm E}, 0\}$, where $C_{\rm B} = \log_2(1+\gamma_{\rm B})$ and $C_{\rm E} = \log_2(1+\gamma_{\rm E})$ are the channel capacities at B and E. Secure transmission holds if $R_{\rm S} \leq C_{\rm S}$; otherwise, a secrecy outage occurs. Thus, the secrecy outage probability (SOP) is SOP = $\Pr\{C_{\rm S} < R_{\rm S}\}$, and a tight lower bound is given by [10]

$$SOP_{L} = \int_{0}^{\infty} F_{\gamma_{B,(\mathcal{P}^{\star})}} \left(2^{R_{S}} \gamma_{E} \right) f_{\gamma_{E,(\mathcal{P}^{\star})}} (\gamma_{E}) d\gamma_{E}. \tag{13}$$

Proposition 2. For FRIS-assisted MISO systems, the SOP_L can be approximated by

$$SOP_L \approx \rho^{k_{\rm B}} \frac{2^{k_{\rm B}R_{\rm S}}}{k_{\rm B} \mathcal{B}(k_{\rm B}, 1)} \, {}_2F_1(k_{\rm B} + 1, k_{\rm B}; 1 + k_{\rm B}; -2^{R_{\rm S}} \rho) \,,$$
(14a)

where, $\rho \triangleq \frac{\overline{\gamma}_{\rm E}\theta_{\rm E}}{\overline{\gamma}_{\rm B}\theta_{\rm B}}$, $\mathcal{B}\left(\cdot,\cdot\right)$ is the beta function, and $_2F_1\left(\cdot,\cdot;\cdot;\cdot\right)$ denotes the Gauss hypergeometric function.

Proof. The result is obtained from [11, Eq. (7)] after appropriate substitutions and mathematical manipulations.

V. NUMERICAL RESULTS AND DISCUSSIONS

This section shows numerical results to validate the analytical framework and assess the secrecy performance of FRIS against conventional RIS schemes. Specifically, two FRIS modes are examined: 1) FRIS with only selected positions optimized (SPO), and 2) FRIS with joint optimization of element positions, transmit BF, and PS (SPO+BF+PS). For comparison purposes, the FRIS is evaluated against two RIS baseline configuration: 1) a Conventional RIS, with M fixed elements positioned at the subregion centers of the FRIS grid, thereby spanning the full aperture area., and 2) a Compact RIS, where M elements form a dense rectangular array with spacing $< \lambda/2$, resulting in a smaller aperture but stronger spatial correlation. For a fair comparison, both RIS baselines employ the same number of elements M as the FRIS and are tested with either random PS or optimized BF and PS. Unless specified otherwise, the FRIS parameters are: carrier frequency $f_c = 2.4$ GHz ($\lambda = 0.125$ m), correlation matrix with $d_{\rm H} = d_{\rm V} = \lambda/3$, aperture size $A_T = 2\,{\rm m}\times 2\,{\rm m}$ $(N_{\rm v}=N_{\rm h}=48)$, path-loss exponents $\beta_1=\beta_i=-40$ dB, secrecy rate threshold $R_{\rm S}=1$ bps/Hz, and $\overline{\gamma}_{\rm E}=12$ dB. The Q-learning algorithm adopts standard parameters: learning rate $\alpha = 0.1$, discount factor $\delta = 0.9$, exploration probability $\epsilon = 0.1$, and E = 400 episodes. For the MLE procedure, $t_{\rm sp} = 10^4$ realizations are used to form the training set in all cases. Monte Carlo simulations over channel realizations are conducted to validate the analysis, while Moment Matching (MoM) is included as a benchmark for SOP approximation.

Figure 2a illustrates the spatial configuration of the FRIS with M=16 fluid elements deployed within a square region. The background grid corresponds to the N uniformly distributed candidate positions, ensuring fine spatial granularity across the surface. The blue markers highlight the active

elements selected by the proposed secrecy-aware optimization framework, while the inactive candidate points are shown in black. From a PLS perspective, this adaptive positioning introduces spatial randomness that increases the eavesdropper's channel uncertainty, effectively reducing the SOP compared to conventional and compact RIS architectures. However, the performance gains become less pronounced when contrasted with fully optimized RIS designs, where BF and PS strategies are employed.

In Fig. 2b, we compare the SOP performance of FRIS with spatial position optimization (SPO) against a conventional RIS with random PS, considering M=36 fluid elements and $L \in \{2,6\}$ transmit antennas. In this setup, neither FRIS nor RIS benefit from BF or PS optimization, thereby isolating the impact of the spatial geometry on the secrecy performance. From a PLS point of view, it is evident that FRIS with optimized positions provides a significant reduction in SOP compared to conventional RIS, especially in the high-SNR regime. This gain comes from the ability of FRIS to introduce spatial randomness, which increases the uncertainty of the eavesdropper's channel. Moreover, as L increases from 2 to 6, the secrecy performance improves notably, confirming that multiple transmit antennas and spatial diversity further enhance PLS. The figure also includes analytical benchmarks such as the Method of Moments (MoM) and the proposed approximation, both of which closely track the simulated SOP, with the proposed approximation exhibiting the best accuracy. These results validate the effectiveness of the proposed model and highlight the advantage of FRIS-assisted systems over conventional RIS in terms of secrecy performance.

In Fig. 2c, we evaluate the SOP performance of FRIS under full optimization, i.e., combined SPO, BF, and PS design, with M=196 fluid elements and L=4 BS antennas. The results are contrasted against multiple benchmarks: a Conventional RIS with random PS, an optimized Conventional RIS (BF+PS), and a Compact RIS (BF+PS). From the curves, it is evident that the optimized FRIS achieves a clear SOP advantage over both the Conventional RIS and the Compact RIS. This gain is particularly notable in the moderate-to-high SNR regime, where the spatial flexibility of FRIS mitigates the correlation losses that limit compact deployments. In contrast, when comparing FRIS with an optimized Conventional RIS (BF+PS), the performance gap becomes marginal, suggesting that once BF and PS are carefully designed, the additional spatial optimization introduced by FRIS provides only limited benefits in terms of SOP. From a PLS standpoint, these findings confirm that the main strength of FRIS lies in scenarios where PS optimization is restricted or impractical, as the spatial adaptation of fluid elements introduces channel randomness that increases the eavesdropper's uncertainty. Meanwhile, the consistent superiority of FRIS over the Compact RIS highlights the importance of spatial diversity and reduced correlation in secrecy-oriented designs.

In Figure 3, we evaluate the SOP performance for both FRIS and conventional RIS under full optimization, considering $L=4,\ M=100,$ and different inter-element spacings between fluid elements. Here, it is observed that by reducing the spacing (e.g., $\lambda/5$) increases the spatial correlation among

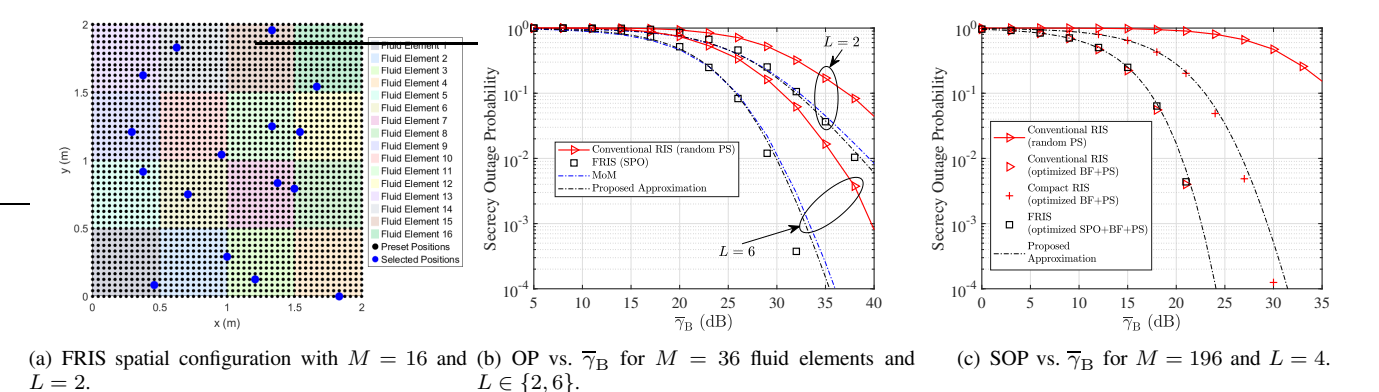


Fig. 2. Spatial configuration and OP achieved for FRIS-aided Multiple-Input Single-Output (MISO). In all figures, the dashed lines represent analytical solutions, while markers correspond to MC simulations. Also, for a fair comparison, the RIS is configured with the same number of elements M as the FRIS in all cases

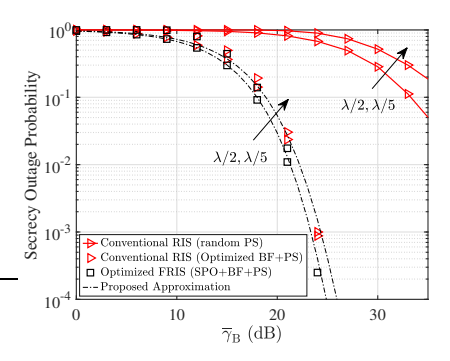


Fig. 3. SOP vs. $\overline{\gamma}_{\rm B}$ for $L=4,\,M=100,$ and different inter-element spacings between fluid elements. Markers denote MC simulations whereas the solid lines represent analytical solutions.

reflecting elements, which in turn reduces the channel diversity and negatively impacts secrecy performance. This effect is clearly visible in the curves, where smaller spacings result in higher SOP values compared to the reference case of $\lambda/2$. Nevertheless, the optimized FRIS (SPO+BF+PS) consistently outperforms the optimized conventional RIS (BF+PS), highlighting that the spatial adaptability of FRIS can mitigate part of the secrecy degradation caused by reduced inter-element distances. In contrast, the conventional RIS with random PS yields the poorest performance due to the absence of any optimization. It is also worth noting that, when both FRIS and conventional RIS employ optimized BF and PS, the additional spatial configuration flexibility of FRIS does not translate into a substantial SOP gain. This observation is consistent with earlier results, confirming that the secrecy benefit of FRIS becomes less pronounced when RIS is already equipped with full optimization. Hence, the main advantage of FRIS lies in scenarios where PS optimization is restricted or impractical, since in such cases spatial adaptability introduces channel randomness that effectively enhances secrecy performance.

VI. CONCLUSIONS

In this work, the SOP performance of FRIS had been investigated and compared with both conventional and compact RIS architectures. It had been shown that the additional degree of freedom introduced by spatial position optimization had allowed FRIS to consistently outperform conventional RIS with random phase shifts, as well as compact RIS, which had suffered from higher spatial correlation and reduced diversity.

Furthermore, results had indicated that FRIS could partially mitigate the secrecy degradation caused by reduced interelement spacing, highlighting its robustness under practical deployment constraints. However, when conventional RIS had been equipped with optimized BF and Ps strategies, the spatial adaptability of FRIS had not provided significant additional SOP gains. Overall, FRIS had demonstrated clear advantages in scenarios where phase optimization was restricted or impractical, thus reinforcing its potential as a promising architecture for enhancing physical layer security.

APPENDIX A PROOF OF PROPOSITION 1

Here, we provide a derivation of the estimation of the distribution parameters of the Nakagami-m model that approximates the PDF of H_i . By considering a training set vector $\mathbf{h}_i^{\star} = \{h_{i,j}^{\star}\}_{j=1}^{t_{sp}}$ obtained from (8), we approximate the PDF of H_i by a Nakagami-m distribution, expressed as

$$f_{H_i}(h; \boldsymbol{\varphi}_i) = \frac{2m_i^{m_i} h^{2m_i - 1}}{\Gamma(m_i) \Omega_i^{m_i}} \exp\left(-\frac{m_i h^2}{\Omega_i}\right), \quad (15)$$

where the parameter vector is $\varphi_i = (m_i, \Omega_i)$. Now, to estimate Ω_i , we substitute (15) into the log-likelihood derivative (10) for the parameter $\varphi_{i,t} = \Omega_i$, which directly leads to the result in (12)a. Similarly, solving (10) with the PDF in (15) for the parameter $\varphi_{i,t} = m_i$ yields

$$\log(m_i) - \psi(m_i) = \underbrace{\log\left[\frac{1}{t_{sp}} \sum_{j=1}^{t_{sp}} (h_{i,j}^{\star})^2\right] - \frac{1}{t_{sp}} \sum_{j=1}^{t_{sp}} \log\left((h_{i,j}^{\star})^2\right)}_{\Delta_i},$$
(16)

where $\psi(\cdot)$ is the digamma function [12, Eq. (6.3.1)]. Since (16) admits no closed-form solution for m_i , we approximate $\psi(\cdot)$ using its asymptotic expansion [12, Eq. (6.3.18)]. By applying a second-order expansion and performing some algebraic manipulations, the closed-form approximation of m_i is obtained as given in (12)b. This completes the proof.

REFERENCES

[1] A. Salem, K.-K. Wong, G. C. Alexandropoulos, C.-B. Chae, and R. Murch, "A first look at the performance enhancement potential of fluid reconfigurable intelligent surface," *IEEE*, 2025.

- [2] J. Zhang et al., "Fluid antenna assisted integrated sensing and communication," IEEE, 2023.
- [3] F. Rostami et al., "Fluid integrated reflecting and emitting surfaces (fires)," IEEE, 2024.
- [4] A. Li et al., "Movable antennas for physical layer security: Principles and performance," *IEEE*, 2023.

 A. Chen *et al.*, "Secrecy outage performance in movable antenna
- systems," IEEE, 2023.
- [6] A. Wang et al., "On the secrecy benefits of movable antennas: A statistical analysis," IEEE, 2024.
- [7] C. J. C. H. Watkins and P. Dayan, "Q-learning," Machine Learning, vol. 8, no. 3-4, pp. 279-292, 1992.
- [8] Q. Wu and R. Zhang, "Intelligent Reflecting Surface Enhanced Wireless Network: Joint Active and Passive Beamforming Design," in 2018 IEEE Global Communications Conference (GLOBECOM), pp. 1-6, 2018.
- [9] M. Blume, "Expectation maximization: A gentle introduction," Technical University of Munich Institute for Computer Science, 2002.
- [10] D. P. M. Osorio, J. D. Vega-Sánchez, E. E. B. Olivo, and A. N. Barreto, "Physical Layer Security," in Security and Privacy Vision in 6G: A Comprehensive Guide (P. Porambage and M. Liyanage, eds.), Wiley-IEEE Press, 2023. First published: 21 July 2023.
- [11] L. Kong, H. Tran, and G. Kaddoum, "Performance analysis of physical layer security over α - μ fading channel," *Electron. Lett.*, vol. 52, no. 1, pp. 45-47, 2016.
- [12] M. Abramowitz and I. A. Stegun, Handbook of Mathematical Functions with Formulas, Graphs, and Mathematical Tables. New York, NY, USA: Dover Publications, 10th ed., 1972.